Science Arts & Métiers (SAM)
is an open access repository that collects the work of Arts et Métiers Institute of Technology researchers and makes it freely available over the web where possible.

This is an author-deposited version published in: https://sam.ensam.eu
Handle ID: .http://hdl.handle.net/10985/22380

To cite this version :

Mohammad SAFEEA, Pedro NETO, Richard BEAREE - An integrated framework for collaborative robot-assisted additive manufacturing - Journal of Manufacturing Processes - Vol. 81, p.406-413 - 2022

Any correspondence concerning this service should be sent to the repository Administrator : scienceouverte@ensam.eu

Journal of Manufacturing Processes xxx (xxxx) 1–8

Contents lists available at ScienceDirect

Journal of Manufacturing Processes

journal homepage: www.elsevier.com/locate/manpro

An integrated framework for collaborative robot-assisted additive manufacturing

Mohammad Safeea [a], Richard Bearee [b], Pedro Neto [a, *]

[a] Centre for Mechanical Engineering, Materials and Processes, University of Coimbra, Coimbra 3030-788, Portugal
[b] Arts et Metiers Institute of Technology, LISPEN, Lille F-59046, France

ARTICLE INFO

Keywords:
Additive manufacturing
Robotics
3D printing

ABSTRACT

Additive manufacturing (AM) is revolutionizing industry, allowing to prototype and fabricate custom-made parts with complex geometries rapidly and at an affordable cost. The use of robots to perform AM has great potentials due to its flexibility and ability to produce multi-directional fabrication paths, conducting to the production of parts that are unachievable using conventional 3-axis machines. In this study, it is proposed a novel multitasking collaborative robot-assisted AM framework featuring the system design, integration, generation of collision free robot paths/motion, robot control and filament extrusion control. Closed loop inverse kinematics was implemented to avoid singularities when generating AM paths for redundant robots featuring null space issues. The orientation control of the robot's end-effector (EEF) allows to eliminate the stair-like structures in fabricated parts by applying finishing layers, and by this way improving the appearance of curved surfaces, improving mechanical properties and better supporting loads in certain directions. Experimental tests carried out on 7-axis redundant robot manipulator show the viability of the system proposed.

1. Introduction

Manufacturing is a driving force for the economy. Due to its importance, an enormous amount of research is dedicated to improving factories' productivity and efficiency. Consequently, new methods have appeared and transformed the way products are made. Lately, Additive Manufacturing (AM) is taking the lead in this advance, and promises to have a huge impact on various domains, namely in manufacturing, biomedical, aerospace and construction industries [1–3].

AM presents various relative advantages in relation to conventional processes (subtractive manufacturing, moulding, etc.) [4], including making prototypes rapidly (from 3D Computer-Aided Design (CAD) to production [5,6]), reducing wasted material and fabricating parts with complex geometries from various materials (metals, plastics, biomaterials, organic cells, or even soft matter). Nevertheless, AM in its diversity of different sub-processes faces some challenges such as the need for post-processing [7,8], defects on produced parts, the need for support structures [9], the on-line adjustment of process parameters, among others. These issues are directly related to the specific AM subprocess and the application.

AM machines with multiple degrees of freedom (DOF), such as robots, bring a number of novel/improved functionalities and challenges to the AM process [10]. Robot-assisted AM technology has its own merits and demonstrated several advantages [11], namely:

1. Production of bigger parts by virtue of the robot's larger working volume (usually larger than conventional AM machines), and which can easily be extended by mounting external motion axes, for example mounting the robot on a moving gantry;
2. The ability to control robot pose (position and orientation), which reflects on the control of the extruder pose while performing AM. The control of the orientation of the extruder promotes the fabrication of parts with better surface appearance, better structural properties (reduce defects and residual stress) and in some cases can eliminate the need to use supporting structures;
3. Multi-directional fabrication and conformal deposition to better support loads in specific directions;
4. The flexibility of the robot itself, which can be re-programmed to be applied on the fabrication of diverse parts using different AM sub-processes.

By virtue of the aforementioned advantages, robot-assisted AM systems are a prominent research topic. Robot technology can expand the capabilities of almost all AM sub-processes [11]. Robotic manipulators

* Corresponding author.
E-mail address: pedro.neto@dem.uc.pt (P. Neto).

https://doi.org/10.1016/j.jmapro.2022.06.067
Received 12 January 2022; Received in revised form 22 June 2022; Accepted 25 June 2022
1526-6125/© 20XX

UNCORRECTED PROOF

Note: Low-resolution images were used to create this PDF. The original images will be used in the final composition.

have been used to print complex 3D geometries without the need for supporting materials [12] or applied for the metal AM directed energy deposition process [13]. However, the integration of robotic and AM systems brings some challenges related to the proper and standard integration of technology, the definition of interconnected robot and AM parameters (collision free paths/motion dealing with surface free stair-like structures) and the on-line control of the entire system, which is especially challenging when robots are redundant and collaborative. In [14], the authors presented a 3D printing system composed of multiple robots working in collaboration, featuring great flexibility in terms of printed geometries, areas and task management. A method to automatically manufacture complex truss structures, using a robot for point-by-point arc additive manufacturing, is presented in [15], where a closed loop control using video feedback from a camera is used to correct for deposition errors. In [16], it is proposed an AM simulator using an off-line robot programming system. While this approach is interesting, it should be noted that the transfer to the real robotic system requires adjustments in diverse parameters related to both robot operation and the AM process itself. Path planning is a key issue in robot-assisted AM, promoting the optimization of accuracy, quality, build time and material use [17]. A recent study proposes an on-line layer height control and an in-process toolpath replanning, enabling better geometric accuracy for tall shell parts [18]. AM path planning has been studied to improve the structural rigidity of produced parts [19].

Robot-assisted AM solutions involve the integration of various hardware and software components. In literature, existing studies on integrated solutions for robot-assisted AM are scarce, even though there is a great demand for them both in academia and industry. Robots allow multiple possibilities in controlling not only the position, but also the orientation of AM extruders, promoting several possibilities regarding fabrication paths (improve mechanical properties, surface appearance, etc.). While there are several different multi-axis approaches to AM, including robot-based solutions, they lack in automatically defining the extruder orientation and related velocity. Usually, the orientation is manually defined or fixed (from surface normal), making the equipment to operate as a 3-axis machine. In such a context, stair-like structures cannot be avoided. Moreover, in many solutions the different elements of software and hardware are not properly integrated, and robots are used as a black box controlled at the end-effector level subject to singularities.

In this paper it is proposed an integrated framework for robot-assisted AM using a collaborative redundant robot performing fused deposition modelling (FDM) as AM sub-process. This is a generic platform that can be easily integrated (hardware and software) in any robot or multi-axis machine featuring position and orientation control in space. Fig. 1 shows the architecture of the proposed framework, featuring the entire process from CAD to production, software and hardware, addressing the above issues of existing multi-axis AM platforms. The functionalities of the Additive Manufacturing Control Software (AMCS) are highlighted, specifically to define collision free robot paths/motion, robot motion control and extruder integrated/coordinated control. The proposed system takes advantage of robot EEF orientation control while

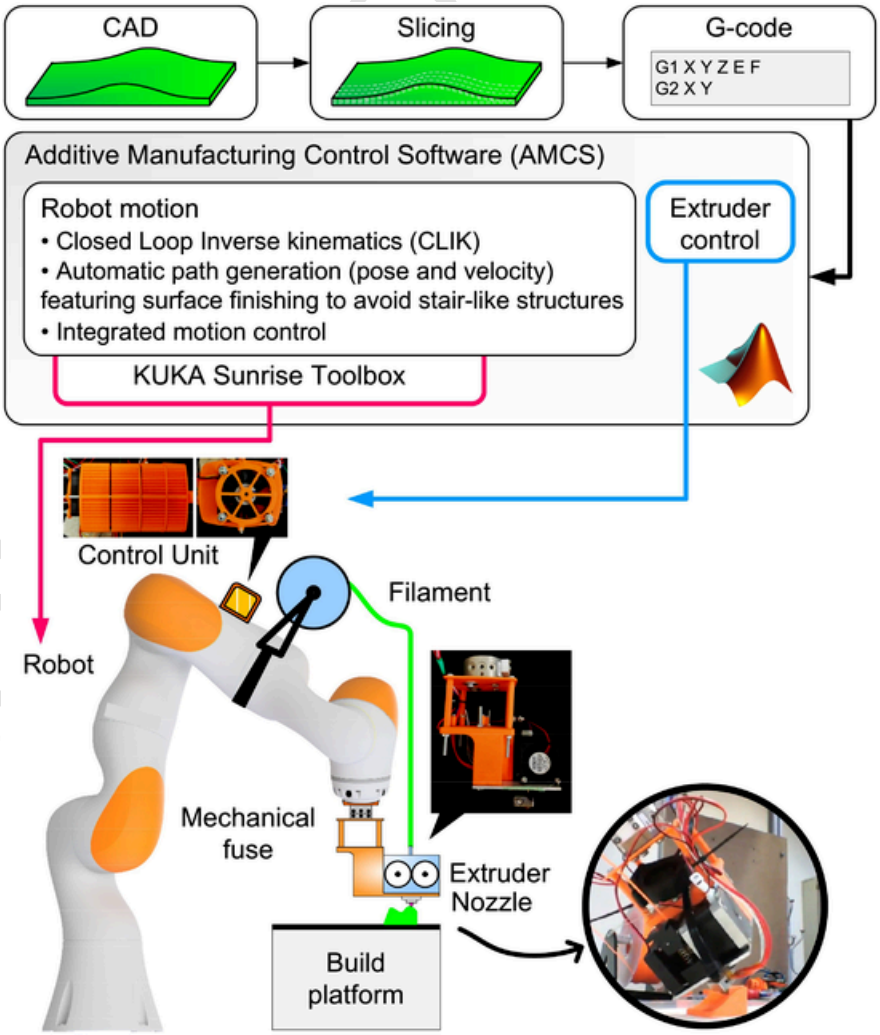

Fig. 1. Integrated robot-assisted AM framework architecture, from CAD to production, software and hardware.

covering the upper surface of the part being produced with a finishing layer (surface contours perpendicular to the structure layers). This layer smooths out (or even eliminates) the stair-like structure, a typical problem in parts produced using conventional 3-axis machines. This is an important step of the path planning process since it reduces the need of post-processing to improve surface appearance and improves the mechanical properties by reducing residual stress. The redundant and collaborative robotic manipulator brings some interesting characteristics to the process, particularly its flexibility, ability to avoid singularities and to work side-by-side with humans. In addition, the AM collaborative robot can be used in other tasks just by changing the extruder and attaching a gripper to it.

The trajectory generation from the EEF path specified in the G-code commands is explained in Section 3. In Section 4, the method used to calculate the robot joints variables (positions and velocities) while avoiding singularities is described. Section 5 explains how to calculate and synchronize the extruder's extrusion rate with the motion of the robot. Section 6 shows the experimental setup of the proposed system and the results of various tests. The conclusion ends the article.

2. Architecture

Starting from the CAD model of the part to fabricate, it is sliced using open-source or propriety software [20] and the G-code commands are generated. The G-code file is read so that the motion parameters are parsed (path coordinates, velocity and extruder control parameters). Those parameters are used afterwards by the proposed AMCS software (written in MATLAB) to control the robot and the extruder, Fig. 1. The AMCS is running on an external Personal Computer (PC), and it is used to perform the computations for the path generation, inverse kinematics, motion control and communicate with the hardware. The main control loop of the AMCS calculates the robot joints velocities and positions required to generate the AM paths at the EEF. This is done using the Closed Loop Inverse Kinematics (CLIK) algorithm [21] on the Cartesian path of the EEF. The control commands for the robot's joints are sent through the Ethernet to the robot controller via the Transmission Control Protocol/Internet Protocol (TCP/IP) recurring to the KUKA Sunrise Toolbox for MATLAB [22]. Simultaneously, the control software calculates the extruder's control commands and streams it to our custom made extruder and it's Control Circuit Unit (CCU), Fig. 2. The CCU consists of a micro-controller board and power electronics, with detailed description in Section 5.

3. Robot path generation

The robot path is first calculated in the Cartesian space according to the G-code commands, distinguishing between linear motion specified by the instruction G1 or circular motion on an arc specified by the instructions G2 and G3 for clockwise and counterclockwise motions, respectively. The generated collision free paths/motion follows a trapezoidal motion profile strategy to deal with the stair-like structures and related robot velocity.

3.1. Linear motion parameterization

The trajectory of a linear motion, for n line segments, is specified by:

$$\boldsymbol{x} = \boldsymbol{x}_0 + \sum_{j=1}^{n} \frac{s_j}{\left\|\boldsymbol{x}_j - \boldsymbol{x}_{j-1}\right\|}\left(\boldsymbol{x}_j - \boldsymbol{x}_{j-1}\right) \tag{1}$$

where the parameter s_j is defined by:

$$s_j = \begin{cases} 0 & 0 \le t \le t_{j-1} \\ f_j(t) & t_{j-1} \le t \le t_j \\ \left\|\boldsymbol{x}_j - \boldsymbol{x}_{j-1}\right\| & t_j \le t \le t_n \end{cases} \tag{2}$$

where $f_j(t)$ is the parametric motion profile along line segment j. A common way to choose this function is to use a trapezoidal motion profile. Consequently, the velocity at the EEF is:

$$\dot{\boldsymbol{x}} = \frac{\dot{s}_j}{\left\|\boldsymbol{x}_j - \boldsymbol{x}_{j-1}\right\|}\left(\boldsymbol{x}_j - \boldsymbol{x}_{j-1}\right) \tag{3}$$

3.2. Circular motion parameterization

For arc motion, data from the G2 and G3 instructions are used. Both instructions are followed by the arc's parameters, from which the center point of the arc $\boldsymbol{c}$ and the end point of the arc $\boldsymbol{p}_e$ are calculated by adding their relative displacements (specified in the G-code) to the Cartesian coordinates of the starting point of the motion $\boldsymbol{p}_0$. Fig. 3 shows the arc and the points $\boldsymbol{c}$, $\boldsymbol{p}_0$ and $\boldsymbol{p}_e$.

After specifying the arc geometrically using the points $\boldsymbol{c}$, $\boldsymbol{p}_0$, $\boldsymbol{p}_e$, the trajectory of the EEF motion along the arc is specified at each instant by calculating the position $\boldsymbol{x}$ and the velocity $\dot{\boldsymbol{x}}$ of the EEF while moving in a circular motion. To do so, an internal motion coordinate system (frame $\mathbf{T}_{arc}$) is specified. The frame $\mathbf{T}_{arc}$ is defined using the arc's parameters $\boldsymbol{c}$, $\boldsymbol{p}_0$ and $\boldsymbol{p}_e$. The center of the arc $\boldsymbol{c}$ is considered as the origin of $\mathbf{T}_{arc}$. However, its bases vectors $\boldsymbol{l}$, $\boldsymbol{m}$ and $\boldsymbol{n}$ are calculated as follows:

- Vector $\boldsymbol{l}$ is a unit vector pointing from the center of the arc to the starting point of the arc $\boldsymbol{p}_0$, thus:

$$\boldsymbol{l} = \frac{\boldsymbol{p}_0 - \boldsymbol{c}}{\left\|\boldsymbol{p}_0 - \boldsymbol{c}\right\|} \tag{4}$$

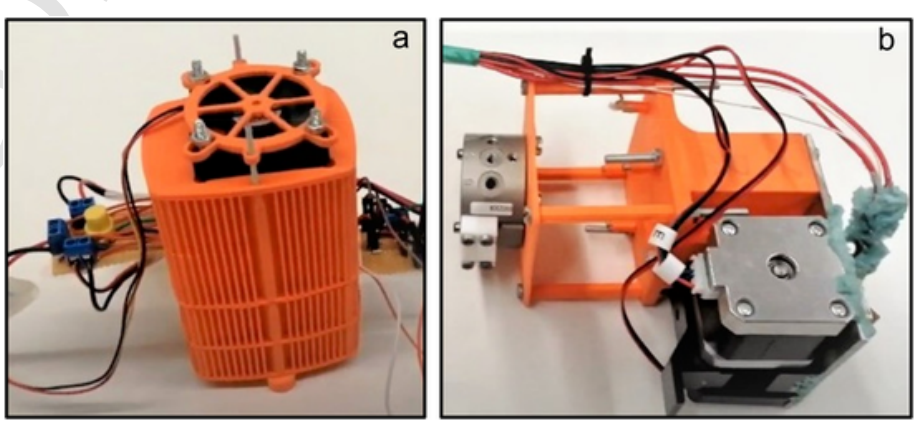

Fig. 2. The extruder's Control Circuit Unit (a) and the extruder's mechanism featuring the mechanical fuse to attach to the robot wrist and nozzle (b).

CORRECTED PROOF

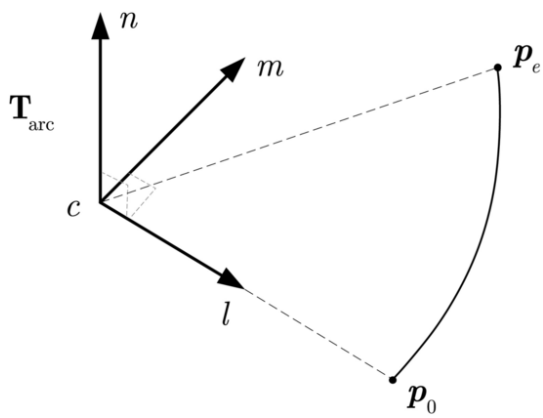

Fig. 3. Circular motion parameterization.

- Based on the G-code instruction the vector $\boldsymbol{n}$ normal to the plane of the arc is already known (perpendicular to the active plane specified by G-code G17, G18 or G19).
- Vector $\boldsymbol{m}$ is calculated using the cross product $\boldsymbol{m} = \boldsymbol{n} \times \mathbf{l}$.

Finally, the position of the EEF $\boldsymbol{x}$ on the arc can be parameterized according to the length of the motion s along the arc while it is performing the circular motion:

$$\boldsymbol{x} = r\left(\cos\left(\frac{s}{r}\right)\boldsymbol{l} + \sin\left(\frac{s}{r}\right)\boldsymbol{m}\right) + \boldsymbol{c} \tag{5}$$

where r is the radius of the arc. The motion parameter s is obtained from the motion profile:

$$s = f(t) \tag{6}$$

Similar to the linear motion, $f(t)$ is the parametric motion profile along the arc. A common way to choose this function is to use a trapezoidal motion profile. Thus, the velocity vector of the EEF during the circular motion is:

$$\dot{\boldsymbol{x}} = \dot{s}\left(\cos\left(\frac{s}{r}\right)\boldsymbol{m} - \sin\left(\frac{s}{r}\right)\boldsymbol{l}\right) \tag{7}$$

After generating the trajectory in the Cartesian space, inverse kinematics is applied to control the robot at the level of the joints as described in Section 4.

4. Closed loop inverse kinematics

The paths calculated in the previous section pertain to the EEF motion in Cartesian space. However, the redundant robot is controlled by actuating its joints, in the joints space. In such a context, it is required to perform the inverse mapping from the EEF position/velocity to the joints position/velocity. This can be done analytically for simple robot structures, or numerically using differential kinematics [21]. A relationship between the EEF linear/angular velocity $\dot{\boldsymbol{x}}$ and the joint velocities $\dot{\boldsymbol{q}}$ through the Jacobian matrix is given by:

$$\dot{\boldsymbol{x}} = \mathbf{J}\dot{\boldsymbol{q}} \tag{8}$$

where, $\mathbf{J}$ is the analytical Jacobian of the robotic manipulator, a $6 \times n$ matrix, where n is the number of the robot's joints. The Jacobian matrix is calculated from:

$$\mathbf{J} = \frac{\delta \boldsymbol{x}'}{\delta \boldsymbol{q}} \tag{9}$$

where $\boldsymbol{x}'$ is the operational space coordinates of the EEF's position and orientation. Thus, the inverse mapping from the EEF linear/angular velocities to the robot joint velocities is achieved by:

$$\dot{\boldsymbol{q}} = \mathbf{J}^{\dagger}\dot{\boldsymbol{x}} \tag{10}$$

where $\mathbf{J}^{\dagger}$ is the pseudo inverse of the Jacobian matrix calculated from $\mathbf{J}^{\dagger} = \mathbf{J}^{\mathrm{T}}(\mathbf{J}\mathbf{J}^{\mathrm{T}})^{-1}$. The angular position of the robot is calculated by integrating with time:

$$\boldsymbol{q} = \int \dot{\boldsymbol{q}}dt \tag{11}$$

However, integrating with time causes accumulative error, which can be corrected by closing the loop in Eq. (10) by using a proportional term:

$$\dot{\boldsymbol{q}} = \mathbf{J}^{\dagger}\left(\dot{\boldsymbol{x}}_{ref} - \mathrm{K}\boldsymbol{e}\right) \tag{12}$$

where, $\dot{\boldsymbol{x}}_{ref}$ is the reference EEF velocity, $\mathbf{K}$ is the proportional gain matrix, a positive definite matrix (usually diagonal), and $\boldsymbol{e}$ is the error in EEF linear/angular position (pose):

$$\boldsymbol{e} = \boldsymbol{x} - \boldsymbol{x}_{ref} \tag{13}$$

where $\boldsymbol{x}_{ref}$ is the reference pose of the EEF and $\boldsymbol{x}$ is the actual pose of the EEF acquired through sensory feedback. This method is known in robotics literature as the first order closed loop inverse kinematics (CLIK) algorithm [21], used to track the reference motion at the velocity level. Controlling the robot using Eq. (12) without further modification might cause problems, especially when the robot moves towards a singular configuration. In such a case, the matrix resulting from the product $\mathbf{J}\mathbf{J}^{\mathrm{T}}$ is singular and $\mathbf{J}^{\dagger}$ does not exist. In a real world scenario, and near a singularity configuration, the joints' velocities increase dramatically, exceeding the physical capacity of the robot and causes an emergency stop. However, using redundancy and by modifying Eq. (12) the robot is able to avoid the singularity while performing the required AM paths, as explained in Section 4.1.

4.1. Null space motion and avoidance of singularity

Redundant robotic manipulators (with more than 6 axis) allow internal self-motion of the robot while maintaining a fixed pose (position and orientation) of the EEF. This type of motion is called the null space motion, and it is done in the null space of the Jacobian matrix:

$$\mathbf{N} = \mathbf{I} - \mathbf{J}^{\mathrm{T}}\left(\mathbf{J}\mathbf{J}^{\mathrm{T}}\right)^{-1}\mathbf{J} \tag{14}$$

where $\mathbf{N}$ is the null space matrix and $\mathbf{I}$ is the identity matrix.

Motion in the null space makes it possible to achieve various secondary objectives without affecting the motion of the EEF on the original 3D printing path. Mathematically, the secondary objective is described by a scalar function $\boldsymbol{\Phi}(q)$, and thus, the resulting joints velocities of the internal self motion are:

$$\dot{\boldsymbol{q}}_{null} = \mathbf{N}\nabla\boldsymbol{\Phi}(q) \tag{15}$$

where $\dot{\boldsymbol{q}}_{null}$ is the resulting angular velocity for the internal self-motion that optimizes the function $\boldsymbol{\Phi}(q)$, and $\nabla\boldsymbol{\Phi}(q)$ is the gradient of $\boldsymbol{\Phi}(q)$. To avoid singularity, a manipulability index [23] is used:

$$\boldsymbol{\Phi}(q) = \sqrt{\det\left(\mathbf{J}\mathbf{J}^{\mathrm{T}}\right)} \tag{16}$$

where *det* is the determinant function. Thus, a CLIK algorithm that is robust to singularities is:

$$\dot{\boldsymbol{q}} = \mathbf{J}^{\dagger}\left(\dot{\boldsymbol{x}}_{ref} - \mathbf{K}\boldsymbol{e}\right) + \mathbf{N}\nabla\boldsymbol{\Phi}(q) \tag{17}$$

CORRECTED PROOF

5. Filament extrusion control

The extrusion rate should be synchronized with the motion of robot's EEF to operate correctly. In our proposed system, this is done by the automatic control of the angular velocity w_{ex} of the extruder's motor. Therefore, the controling program on the computer side calculates w_{ex} according to both (1) the extrusion length in the G-code command and (2) the trajectory of the motion. Typical G-code commands are:

```
G1 X117.7 Y111.8 E31.5
G1 X82.29 Y112.1 E34.7
```

G1 defines linear motion, followed by the x, y and z coordinates of the target point. In the example above z is omitted, signifying that there is no change in the z coordinate (motion is on the xy plane). The G-code also contains the parameter E for the total extrusion length of the filament. In the previous G-code example, the EEF moves along the x and y axes, and at the same time the extruder consumes a length of the filament equal to $\Delta E = 34.7 - 31.5 = 3.2$ [mm]. To achieve w_{ex}, at first the rate of filament consumption $\dot{E}$ is calculated:

$$\dot{E} = \frac{\Delta E}{s} v \tag{18}$$

where v is the linear velocity of the 3D printing motion of the EEF and s is the length of the motion of the EEF. Therefore, for the G1 command s is the length of the line specified by the command (Euclidean distance). On the other-hand, for G2/G3 commands, the parameter s is the length of the arc specified by the command. Calculating $\dot{E}$ through Eq. (18) allows on-the-fly readjustment of the extrusion rate when overriding the Cartesian velocity of the EEF. Consequently, allowing a rapid readjustment for the 3D printing parameters.

Based on $\dot{E}$, the control program calculates the angular velocity w_{ex} of the extruder motor:

Table 1
Extruder components.

Item	Description
Stepper motor	Pull the filament
Heating coil	Heat the filament
Thermistor	Measure the temperature
Micro-controller	Control the stepper motor and the heater
IRF520	Switch the power to the heater
L298N	H bridge to provide the driving current for the stepper motor

$$w_{ex} = \frac{\dot{E}}{r_w} \tag{19}$$

where r_w is the radius of the friction wheel used to pull in the filament. The friction wheel is connected directly to the motor's shaft. The control program on the PC side calculates w_{ex} and streams it to the micro-controller through serial communication. The micro-controller uses w_{ex} as a reference command for the low level control of the angular velocity of the extruder motor.

6. Experimental setup and results

The proposed framework is composed by an extruder (3D printing head) equipped with a custom-made low-cost driving circuit, a redundant collaborative robot and a PC running the AMCS software, Fig. 1.

The various components used for the extruder and the driving circuit are listed in Table 1, and the circuit diagram is in Fig. 4. A micro-controller (Arduino UNO) is used to control the extrusion rate and the extruder's temperature. Using its Analog to Digital Converter (ADC) pin, the micro-controller acquires feedback on the extruder's temperature from a resistor bridge containing the thermistor. The micro-controller calculates the temperature of the extruder from the voltage measured, by interpolation using a voltage/temperature table. Depending on the temperature registered, the micro-controller switches the power to the heating coil through the IRF520 MOSFET transistor. Also, the micro-controller is used to control the rate of extrusion by commanding the stepper motor through the driving circuit L298N, which contains two H bridges to provide the current to the coils of the stepper motor.

The robot is a 7 DOF redundant KUKA iiwa manipulator (both models 7R800 and 14R820 were used). Using a redundant robot offers various advantages, the most relevant to our system include (1) singularity avoidance and (2) joint limits avoidance. The KUKA Sunrise Toolbox (KST) [22] is used to interface with the robot from an external computer.

The AMCS software, in addition to its features related to the generation of AM robot paths, robot motion control and extruder control, exchanges data with the robot (Ethernet) and with the extruder micro-controller board (serial communication). A low-level control program (written in C) is implemented on the micro-controller. This program is used to control the temperature of the extruder at the required value (around 210 degrees Celsius for Polylactic Acid (PLA) filament). It is also used to control the extrusion rate at the reference value received

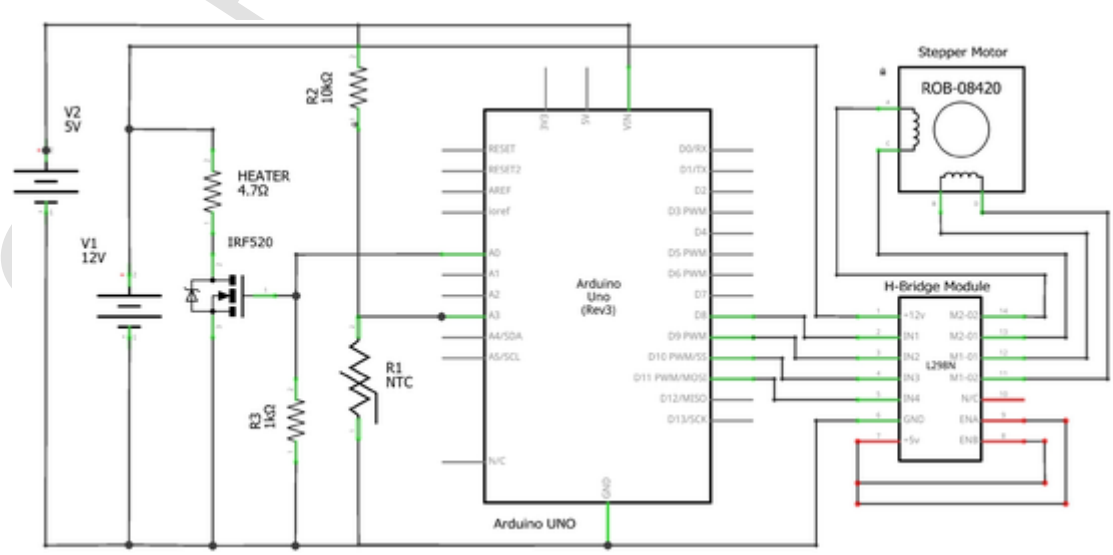

Fig. 4. Diagram for the extruder driving circuit.

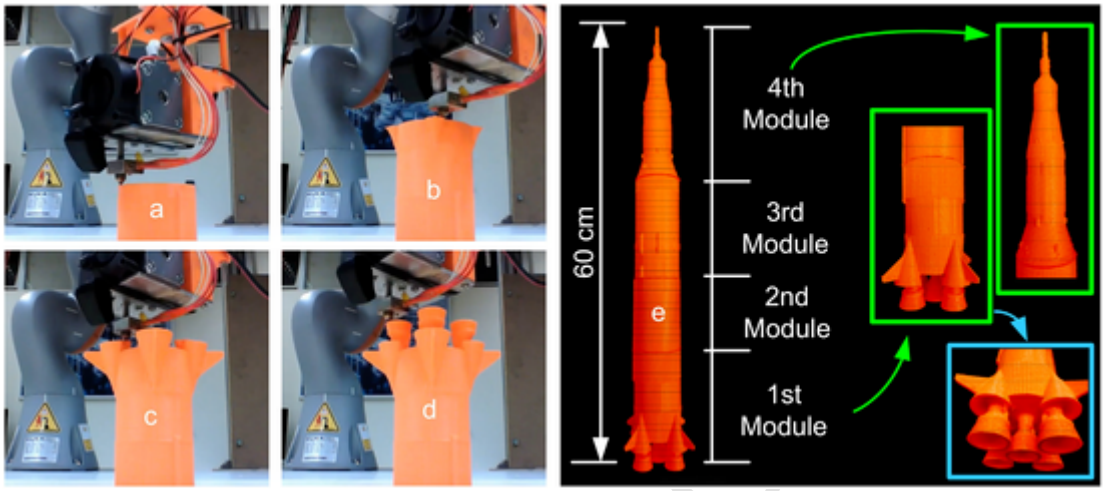

Fig. 5. Robot-assisted AM fabrication of the first module of the space rocket Saturn V (a-d) and the 4 modules assembled (e).

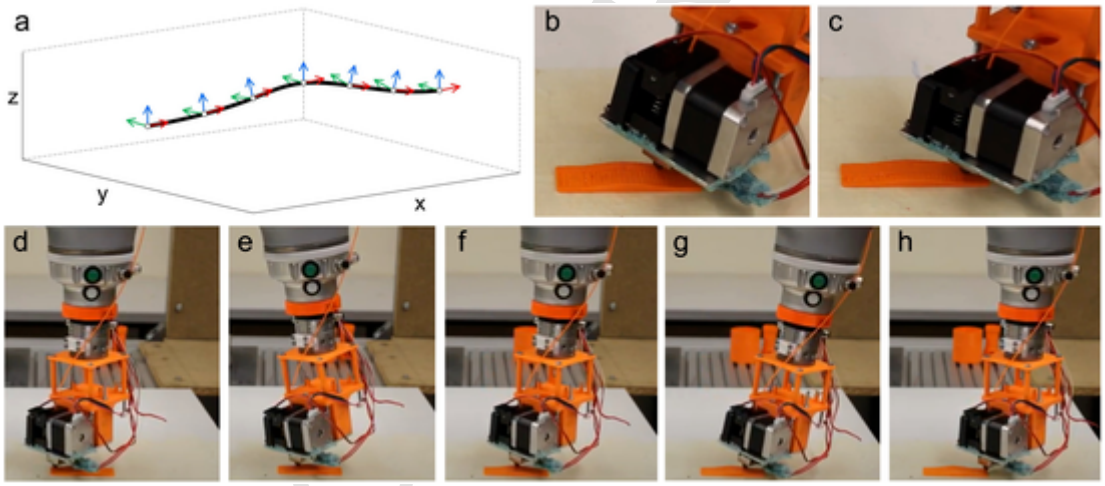

Fig. 6. AM curved path in 3D space with orientation changes (a) and the robot applying the finishing layer by taking advantage of the robot's EEF orientation control (b-h).

from the AMCS. The extrusion rate is synchronized with the motion of the robot.

6.1. Test 1

In Test 1, the proposed AM framework was used to fabricate various parts using PLA filament (1.75 mm and 3 mm diameter) and a 0.8 mm diameter nozzle. The parts were fabricated in horizontal layers, without taking advantage of the EEF orientation control. Fig. 5 shows the fabrication of different parts composing a space rocket (from CAD model of Saturn V). It is demonstrated that the proposed framework can successfully produce such type of parts, featuring geometrical complexity and surface appearance quality. The video in multimedia materials shows the process.

6.2. Test 2

In Test 2, the proposed AM framework takes advantage of the robot's EEF orientation control to cover the upper surface of the part with a finishing layer where the surface contours are perpendicular to the structure layers, Fig. 6. The curve profile of the part's cross-section is defined by:

$$z = z_0 \exp\left(\frac{-y^2}{\beta^2}\right) \tag{20}$$

where $z_0 = 3$ mm and $\beta = 18$ mm. The part's length is made parallel to the y axis of the robot's base and its width is made parallel to the x axis of the robot base, making the calculation of the EEF's orientation and its angular velocity simpler. The EEF's orientation is $(0, \alpha, 0)$ in the ZYX Euler angles convention, where α is given by:

$$\alpha = \pi - \arctan\left(\frac{dz}{dy}\right) \tag{21}$$

The finishing layer eliminates the stair-like structure, a typical problem in parts produced using conventional 3-axis machines. Fig. 7 shows a comparison of a 3D part printed by a conventional 3-axis printing machine (a) and the same part produced using the proposed framework featuring a finishing layer (b). Experimental tests are illustrated in the video in multimedia materials.

The application of the finishing layer reduces the need of post-processing to improve surface appearance (avoid stair-like appearance). Moreover, it improves the mechanical properties of the parts by reducing residual stress and better supporting loads in certain directions. A 3-point bend test demonstrated that part strength is improved in about 25 % by applying the finishing layer, Fig. 8. Two specimens

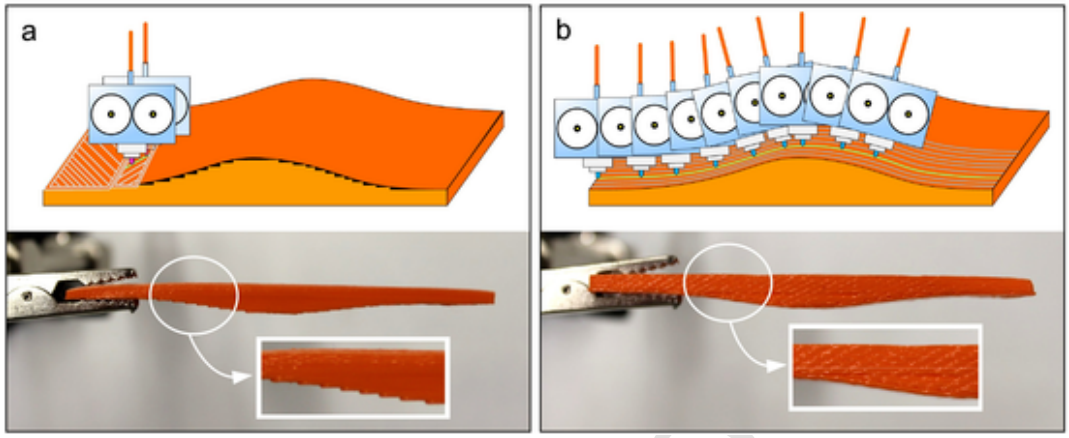

Fig. 7. Stair-like phenomenon when the part is fabricated in a conventional 3-axis AM machine without orientation control (a) and the smoother surface when covered with the finishing layer using the robot's orientation control to avoid stair-like appearance (b).

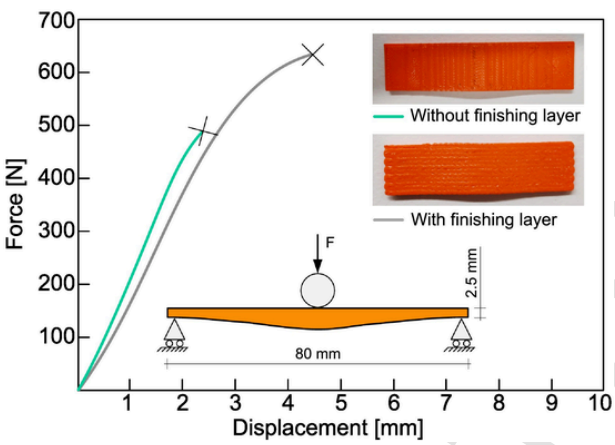

Fig. 8. Three-point bend test where the prescribed displacement of the loading pin increases until the fracture of the specimen.

were considered in this test, one with finishing layer (mass of 4.5 g) and the other without finishing layer (mass of 4 g). The prescribed displacement of the loading pin increases until the fracture of the specimen.

6.3. Discussion

In both tests, the pose error that may exist is from the robot itself or from the calibration of the robot. AM deposition paths featuring position and orientation are automatically extracted from CAD, as in conventional AM processes. In Test 1, it was demonstrated that the proposed system can produce parts as a conventional 3-axis machine. Its working volume is relatively large since it is only limited by the working volume of the robot being used. In Test 2, the robot's EEF orientation control demonstrated effective to apply finishing layers in curved surfaces, eliminating the stair-like structure and improving part's strength in 25 %. Such curved paths are automatically extracted from CAD, defined by the AMCS and applied by the robot. In both tests, the AMCS software demonstrated versatile to generate robot paths and control the main parameters of the AM process together with the robot (including singularities avoidance) and the extruder.

7. Conclusion

This study presented a framework for robot-assisted AM, featuring both software and hardware, from the CAD model to the final production of the part. It was demonstrated its effectiveness in producing quality parts of different dimensions and geometries. The implementation of the closed loop inverse kinematics on the redundant robot allowed singularity avoidance. Controlling the robot's EEF orientation makes it possible to produce better quality parts without the stair-like structure on their surface finish, improving the appearance, improving mechanical properties (25 % in part's strength) and better supporting loads in certain directions. Motivated by various requests from both academia and industry, ongoing and future work is related to the implementation of the system on different robotic systems and industry domains.

Supplementary data to this article can be found online at https://doi.org/10.1016/j.jmapro.2022.06.067.

Declaration of competing interest

The authors declare that they have no known competing financial interests or personal relationships that could have appeared to influence the work reported in this paper.

Acknowledgment

This research was partially supported by Fundação para a Ciência e a Tecnologia COBOTIS (PTDC/EME-EME/32595/2017), UIDB/00285/2020, and UE/FEDER through the program COMPETE 2020 PRODUTECH4S&C (46102).

References

[1] Kumar R, Kumar M, Chohan J.S. The role of additive manufacturing for biomedical applications: a critical review. J Manuf Process 2021;64:828–50. https://doi.org/10.1016/j.jmapro.2021.02.022. https://www.sciencedirect.com/science/article/pii/S1526612521001080.

[2] Gisario A, Kazarian M, Martina F, Mehrpouya M. Metal additive manufacturing in the commercial aviation industry: a review. J Manuf Process 2019;53:124–49. https://doi.org/10.1016/j.jmsy.2019.08.005. https://www.sciencedirect.com/science/article/pii/S0278612519300731.

[3] Freire B, Babcinschi M, Ferreira L, Señaris B, Vidal F, Neto P. Direct energy deposition: a complete workflow for the additive manufacturing of complex shape parts. URL. Procedia Manuf 2020;51:671–7. https://doi.org/10.1016/j.promfg.2020.10.094. https://www.sciencedirect.com/science/article/pii/S235197892031951X.

[4] Guo N, Leu M.C. Additive manufacturing: technology, applications and research needs. Front Mech Eng 2013;8(3):215–43.

[5] Zhang B, Goel A, Ghalsasi O, Anand S. Cad-based design and pre-processing tools for additive manufacturing. URL. J Manuf Syst 2019;52:227–41. https://doi.org/10.1016/j.jmsy.2019.03.005. https://www.sciencedirect.com/science/article/pii/S0278612519300160.

[6] Nurhudan A.I, Supriadi S, Whulanza Y, Saragih A.S. Additive manufacturing of metallic based on extrusion process: a review. J Manuf Process 2021;66:228–37. https://doi.org/10.1016/j.jmapro.2021.04.018. https://www.sciencedirect.com/science/article/pii/S1526612521002553.

[7] Li L, Haghighi A, Yang Y. A novel 6-axis hybrid additive-subtractive manufacturing process: design and case studies. J Manuf Process 2018;33:150–60. https://doi.org/10.1016/j.jmapro.2018.05.008. https://www.sciencedirect.com/science/article/pii/S1526612518304602.

[8] Shakil S.I, Smith N.R, Yoder S.P, Ross B.E, Alvarado D.J, Hadadzadeh A, et al. Post fabrication thermomechanical processing of additive manufactured metals: a review. J Manuf Process 2022;73:757–90. https://doi.org/10.1016/j.jmapro.2021.11.047. https://www.sciencedirect.com/science/article/pii/S1526612521008549.

[9] Jiang J, Xu X, Stringer J. Support structures for additive manufacturing: a review. J Manuf Mater Process 2018;2(4). https://doi.org/10.3390/jmmp2040064. https://www.mdpi.com/2504-4494/2/4/64.

[10] Jiang J, Newman S.T, Zhong R.Y. A review of multiple degrees of freedom for additive manufacturing machines. URL. Int J Comput Integr Manuf 2021;34(2): 195–211. https://doi.org/10.1080/0951192X.2020.1858510. https://doi.org/10.1080/0951192X.2020.1858510.

[11] Bhatt P.M, Malhan R.K, Shembekar A.V, Yoon Y.J, Gupta S.K. Expanding capabilities of additive manufacturing through use of robotics technologies: a survey. Addit Manuf 2020;31:100933. https://doi.org/10.1016/j.addma.2019.100933. https://www.sciencedirect.com/science/article/pii/S2214860419312266.

[12] Laarman J, Jokic S, Novikov P, Fraguada L.E, Markopoulou A. In: Anti-gravity Additive Manufacturing, Fabricate 2014: Negotiating Design & Making; 2014. p. 191–7.

[13] Ding Y, Warton J, Kovacevic R. Development of sensing and control system for robotized laser-based direct metal addition system. Addit Manuf 2016;10:24–35. https://doi.org/10.1016/j.addma.2016.01.002. https://www.sciencedirect.com/science/article/pii/S2214860416300148.

[14] Shen H, Pan L, Qian J. Research on large-scale additive manufacturing based on multi-robot collaboration technology. Addit Manuf 2019;30:100906. https://doi.org/10.1016/j.addma.2019.100906. https://www.sciencedirect.com/science/article/pii/S2214860419308243.

[15] Radel S, Diourte A, Soulié F, Company O, Bordreuil C. Skeleton arc additive manufacturing with closed loop control. Addit Manuf 2019;26:106–16. https://doi.org/10.1016/j.addma.2019.01.003. https://www.sciencedirect.com/science/article/pii/S2214860418305141.

[16] Zhang G.Q, Spaak A, Martinez C, Lasko D.T, Zhang B, Fuhlbrigge T.A. Robotic additive manufacturing process simulation-towards design and analysis with building parameter in consideration. In: 2016 IEEE international conference on automation science and engineering (CASE). IEEE; 2016. p. 609–13.

[17] Jiang J, Ma Y. Path planning strategies to optimize accuracy, quality, build time and material use in additive manufacturing: a review. Micromachines 2020;11(7). https://doi.org/10.3390/mi11070633. https://www.mdpi.com/2072-666X/11/7/633.

[18] Ščetinec A, Klobčar D, Bračun D. In-process path replanning and online layer height control through deposition arc current for gas metal arc based additive manufacturing. J Manuf Process 2021;64:1169–79. https://doi.org/10.1016/j.jmapro.2021.02.038. https://www.sciencedirect.com/science/article/pii/S1526612521001249.

[19] Sales E, Kwok T.-H, Chen Y. Function-aware slicing using principal stress line for toolpath planning in additive manufacturing. J Manuf Process 2021;64:1420–33. https://doi.org/10.1016/j.jmapro.2021.02.050. https://www.sciencedirect.com/science/article/pii/S1526612521001523.

[20] Babcinschi M, Freire B, Neto P, Ferreira L.A, Señaris B.L, Vidal F. Automationml for data exchange in the robotic process of metal additive manufacturing. In: 2019 24th IEEE international conference on emerging technologies and factory automation (ETFA). IEEE; 2019. p. 65–70.

[21] Siciliano B. A closed-loop inverse kinematic scheme for on-line joint-based robot control. Robotica 1990;8(3):231–43.

[22] Safeea M, Neto P. Kuka sunrise toolbox: interfacing collaborative robots with matlab. IEEE Robot Autom Mag 2019;26(1):91–6.

[23] Yoshikawa T. Manipulability of robotic mechanisms. Int J Robot Res 1985;4(2): 3–9.

CORRECTED PROOF